Dynamic saturation optical microscopy: employing dark-state formation kinetics for resolution enhancement

Jana Humpolíčková,*[a] Aleš Benda,[a] Radek Macháň,[a] Jörg Enderlein[b] and Martin Hof[a]

Received 29th March 2010, Accepted 14th July 2010
DOI: 10.1039/c0cp00059k

Fluorescence microscopy has become one of the most rapidly developing observation techniques in the field of molecular biology, since its high sensitivity, contrast and labeling specificity together with being non-invasive fulfill the most important requirements of live cell imaging. The biggest limitation of the technique seems to be the spatial resolution which is, based on Abbe's diffraction law, restricted to some hundreds of nanometres. Recently, various approaches have been developed that overcome the limit imposed by the diffraction barrier and these methods currently lead the development in the field of fluorescence microscopy. In this contribution, we present dynamic saturation optical microscopy (DSOM)—a new technique that monitors the temporal decay of the excited singlet state due to a dark state formation. By mapping the intensity dependent decay kinetics, enhanced resolution images can be obtained. Generally, any dark state of fluorescent molecules can be employed in DSOM. Here, we focus our attention on triplet state formation.

Introduction

Fluorescence microscopy has become one of the most powerful imaging techniques, which is widely used in biology. It is characterized by an unsurpassed sensitivity down to the imaging of individual molecules, and by a high image contrast together with the fact that it allows for highly specific labeling. Fluorescence microscopy employs non-invasive visible light which is advantageous when imaging living systems at ambient conditions as it causes minimum damage. However, its spatial resolution capability is restricted by the diffraction of light as described by Abbe's famous law, limiting the image resolution to some hundreds of nanometres depending on the wavelength and numerical aperture of the objective lens.

The past decade has seen a revolution in pushing down the resolution limit of far-field fluorescence microscopy. This was achieved by the invention and further development of a large variety of different methods. Most of these approaches are based on one or several of the following techniques: (i) non-uniform illumination of the sample, (ii) saturation of the excited state, and (iii) employment of dark states (off-state) of the fluorescent labels. The non-uniform illumination, or so called "structured illumination",[1] increases the amount of spatial frequencies in the Fourier space and thus acts like if the numerical aperture of the objective was larger. The two-fold improvement in resolution which can be achieved with structured illumination can be further increased when optical saturation of the transition between ground and excited states is invoked.[2] Except for saturating structured excitation, which was shown in the wide-field mode of illumination, two more approaches using the saturation in the confocal mode of illumination were introduced: saturation excitation microscopy,[3] analyzing the higher order harmonics arising upon temporally modulated excitation, and direct measurement of the saturation curve at every scanning step.[4] The third group of techniques based on the switching of fluorescent molecules between on- and off-states seems to be the most powerful in terms of resolution. Stimulated emission depletion (STED) microscopy, working in laser scanning mode, uses a donut-shaped depletion laser to switch molecules on the edges of the excitation volume to the off-state and thus precisely localizes only those that remain in the on-state. It has been shown that there is no longer any principal resolution barrier since spatial resolution can approach infinity by correspondingly increasing the power of the depletion light. It was shown experimentally that nitrogen vacancies in nanodiamonds can be visualized with sub-nanometre resolution,[5] which means that the only limiting factor is the size of the observed structure. To improve the axial resolution, combination of two opposing lenses has to be employed.[6] In the case of wide field microscopy, the idea of switching between two states has been used for stochastic optical reconstruction microscopy (STORM)[7–9] and photo-activation localization microscopy (PALM). Photoactivable proteins or stochastically activated organic dye molecules[10,11] are excited in such a way that there is always a maximum of one fluorophore excited within a diffraction-limited area of detection. The photons obtained from the fluorophore before it re-enters the off-state are used for high-precision positioning of the molecule. The resolution of the final image reconstructed from mapping many fluorophores' positions was shown to be around 20 nm. Recently, a 3D super-resolution optical fluctuation imaging (SOFI)[12] has been introduced, a method that analyzes amplitudes of higher order temporal correlations of signal caused by fluorescence blinking during a sequence of images. The method is supposed to reach a 5-fold

[a] *J. Heyrovský Institute of Physical Chemistry of the Academy of Sciences of the Czech Republic, v. v. i. Dolejškova 3, Prague 8, 18223, Czech Republic. E-mail: jana.humpolickova@jh-inst.cas.cz*
[b] *III. Institute of Physics, Georg-August-Universität Göttingen, Friedrich-Hund-Platz 1, 37077, Göttingen, Germany*

resolution improvement with a conventional wide-field microscope.

In this manuscript, we present an experimental realization of a new technique, dynamic saturation optical microscopy (DSOM). Even though the method was theoretically introduced already in 2005,[13] its experimental applicability has not been shown so far. DSOM relies on the dynamic transition between on- and off-states and is based on spatial monitoring of the transition kinetics. The basis of DSOM lies in the fact that the temporal decay of the average fluorescence intensity upon discontinuous excitation exhibits an exponential behavior due to transitions into a dark state. The larger the excitation intensity, the faster the transition into the dark state takes place, leading to a faster exponential decay of the fluorescence signal. This can be used for enhancing spatial resolution. Since DSOM maps different kinetics at places of different illumination, it can be straightforwardly combined with confocal microscopy, as will be reported here. However, it could be also implemented into a wide-field microscope using structured illumination.

The dark state required for DSOM can be realized by employing any reversibly photoswitchable fluorophores (*e.g.* photoswitchable proteins) or by the transition to the triplet state. The advantage of the latter approach is that the ability to switch into a triplet state (intersystem crossing) is common for the majority of fluorophores. In this contribution, we focus on the triplet state transition and discuss the requirements needed for its successful application to DSOM.

The method was tested on two model systems: (i) labeled supported lipid bilayers (SLBs) and (ii) labeled 100 nm polystyrene particles dispersed on a surface. The main reason for choosing SLBs is to show the applicability of DSOM in the case where photobleaching of the dye is not a limiting factor for data quality. In SLBs, the labeled lipid molecules freely diffuse in the bilayer and continuously recover the photobleached load of the labels in the illuminated spot. As the thickness of the layer (around 5 nm) is infinitesimally smaller than the axial extent of the detection region, we can use SLBs to show the resolution enhancement along the optical axes. In the case of fluorescent beads, we demonstrate that reasonable resolution enhancement can be obtained even when photobleaching becomes an issue.

The main advantage of DSOM compared to other methods mentioned above is that it works without requiring a complex optical setup or difficult mathematical treatment.

Results and discussion

Theory

Even though the concept of DSOM only requires spatially inhomogeneous distribution of excitation light, which can be realized both in the widefield and confocal modes of imaging, all our experiments make use of naturally uneven light distribution in a tightly focused laser beam of the confocal microscope. Therefore, a typical imaging procedure is realized by pixel-by-pixel scanning of a specimen. At every position of the scanner, a microsecond laser pulse is generated, which causes (i) a fast pre-equilibrium between the S_0 and S_1 state of the fluorophore and (ii) a decay of the singlet state and therefore also fluorescence due to a triplet state formation. As shown further, the rate of the temporal drop is excitation intensity dependent. Therefore the transition rate at every pixel specifies the position of the fluorophore within the laser focus. To detect the fast decay, EM-CCD camera is employed in a special mode that allows for the necessary temporal resolution.

As having been shown elsewhere,[4] the formation of the excited singlet state and consecutive transition to the triplet state occur on different timescales and therefore the formation of the excited singlet state and the kinetics of the triplet state formation can be treated independently. Consider a sample that is illuminated by a constant light intensity, that was suddenly switched on at time $t = 0$. The dependence of the steady-state probability of finding a molecule in the excited state S_1 (provided that no triplet is formed) on the excitation rate k_{ex} is:

$$S_1\left(t \gg \frac{1}{k + k_{ex}}\right) = \frac{\frac{k_{ex}}{k}}{1 + \frac{k_{ex}}{k}} = K, \qquad (1)$$

where k is the rate constant of the excited singlet-to-ground state transition (fluorescence). This steady state is reached already after few nanoseconds and provides the initial condition for the subsequent triplet state formation which occurs on the microsecond timescale τ. The evolution of the probability that a molecule is in the triplet state T is described by the equation:

$$\frac{dT(\tau)}{d\tau} = k_{isc}S_1(\tau) - k_{rel}T(\tau), \qquad (2)$$

where k_{isc} is the intersystem crossing rate constant and k_{rel} is the triplet state relaxation rate constant. The probability of having a molecule in the S_1 state on the microsecond timescale is a product of the steady-state probability of S_1 given by eqn (1) and the probability function $\alpha(\tau)$, which describes the depopulation of both the singlet ground and excited states. The probability of finding a molecule in the S_1 state is therefore: $S_1(\tau) = \alpha(\tau)K$. Taking into account the fact that one has always $\alpha(\tau) + T(\tau) = 1$, the temporal fading of the S_1 state at time τ after the laser has been turned on is the following:

$$S_1(\tau) = K\frac{k_{rel} + k_{isc}Ke^{-(k_{rel}+k_{isc}K)\tau}}{k_{rel} + k_{isc}K}. \qquad (3)$$

If a fluorescent pattern given by a spatial distribution of fluorophores' concentration $c(\boldsymbol{r})$ is scanned with a tightly focused laser beam, giving rise to an inhomogeneous field of excitation rates $k_{ex}(\boldsymbol{r})$, the acquired spatio-temporal image $\mathrm{im}(\boldsymbol{r},\tau)$ becomes a convolution of the pattern $c(\boldsymbol{r})$ and the spatial profile of the temporally evolving probabilities $S_1(\boldsymbol{r},\tau)$:

$$\mathrm{im}(\vec{r},\tau) = k\int d\vec{r}'c(\vec{r}')S_1(\vec{r} - \vec{r}',\tau). \qquad (4)$$

For the sake of simplicity, eqn (4) assumes that the collection efficiency function is uniform, *i.e.* there is no effect of a pinhole.

After insertion of eqn (3) into eqn (4), the spatio-temporal image of the observed fluorescence pattern becomes:

$$\mathrm{im}(\vec{r},\tau) = I_{\mathrm{stac}}(\vec{r}) + k\int \mathrm{d}\vec{r}\,' c(\vec{r}-\vec{r}\,')K(\vec{r}\,') \times \left(1-\frac{k_{\mathrm{rel}}}{k_{\mathrm{T}}(\vec{r}\,')}\right)\mathrm{e}^{-k_{\mathrm{T}}(\vec{r}\,')\tau}. \quad (5)$$

The temporally independent part of the expression, I_{stac}, equals:

$$I_{\mathrm{stac}}(\vec{r}) = k\int \mathrm{d}\vec{r}\,' c(\vec{r}-\vec{r}\,')K(\vec{r}\,')\frac{k_{\mathrm{rel}}}{k_{\mathrm{T}}(\vec{r}\,')}. \quad (6)$$

k_{T} is the intensity dependent rate constant of the S_1 to triplet transition: $k_{\mathrm{T}}(\vec{r}) = k_{\mathrm{rel}} + k_{\mathrm{isc}}K(\vec{r})$. The calculation of the finite integral in eqn (5) can be performed as an infinite sum of contributions with a given value of k_{T}. Mathematically it means expanding the expression using a delta function: $\delta(k_{\mathrm{T}}(\vec{r}) - k_{\mathrm{rel}} - k_{\mathrm{isc}}K(\vec{r}))$ with a center position at the given value k_{T}. Eqn (5) can be rewritten as:

$$\mathrm{im}(\vec{r},\tau) = I_{\mathrm{stac}}(\vec{r}) + k\int_{k_{\mathrm{rel}}}^{k_{\mathrm{rel}}+k_{\mathrm{isc}}\max(K(\vec{r}))} \mathrm{d}k_{\mathrm{T}} A(k_{\mathrm{T}}|\vec{r})\mathrm{e}^{-k_{\mathrm{T}}(\vec{r})\tau}, \quad (7)$$

where

$$A(k_{\mathrm{T}}|\vec{r}) = \int \mathrm{d}\vec{r}\,' c(\vec{r}-\vec{r}\,')K(\vec{r}\,') \times \left(1-\frac{k_{\mathrm{rel}}}{k_{\mathrm{T}}(\vec{r}\,')}\right)\delta(k_{\mathrm{T}}(\vec{r}\,') - k_{\mathrm{rel}} - k_{\mathrm{isc}}K(\vec{r}\,')). \quad (8)$$

The delta function defines places with the same value of the kinetic constant k_{T}, which can be understood as "iso-kinetic" curves and spheres in the inhomogeneous 2D and 3D field of excitation light, respectively. Position of a fluorophore in the map of the "iso-kinetics", which can be accessed by introducing fluorescence dynamics, can generally generate resolution that is higher than the resolution given by the diffraction limit. The precision of the localization depends on the resolution of k_{T} values, which is given by the temporal resolution of the dynamic experiment and by the number of photons that are collected.

Eqn (7) says that the final spatio-temporal image can be treated as an infinite sum of spatial contributions $A(k_{\mathrm{T}}|\vec{r})$ that associate with the particular value of k_{T}. Since the "iso-kinetics" are only defined by the photochemical characteristics of the fluorophore and by the local excitation power, apparently in the case of confocal imaging with a 2D-Gaussian beam profile, the "iso-kinetic" curves would be infinitely thin concentric circles, where the fastest "iso-kinetic" curve would have an infinitely small radius, which results in the fact that DSOM has no theoretical resolution limit. If the infinite sum is approximated by a finite sum of n exponentials:

$$\mathrm{im}(\vec{r},\tau) \approx \sum_{i=1}^{n} A(k_{\mathrm{T}} \in \langle k_{\mathrm{T}_i}, k_{\mathrm{T}_i} + \Delta k_{\mathrm{T}}\rangle|\vec{r})\mathrm{e}^{-k_{\mathrm{T}_i}\tau}\Delta k_{\mathrm{T}} + A(\vec{r}), \quad (9)$$

($A(\boldsymbol{r})$ is the temporally constant offset) the spatial contributions $A(k_{\mathrm{T}_i}|\vec{r})$ to the 2D PSF become rings of definite thickness, where the radius of the central spot corresponding to the fastest kinetics defines the obtainable resolution (see Fig. 1). When we discuss treatment of the experimental data further in the manuscript, we will show that two exponentials, *i.e.* $n = 2$, is sufficient.

When designing the DSOM experiment, several facts have to be considered:

Amount of the temporally constant offset. Fig. 1 shows an example experiment where the amplitude of the kinetic part of the decay was more than 50% of the entire fluorescence signal. This, however, does not have to be always the case. The relative amplitude a_{rel} of the kinetic part of the decay curve is given by:

$$a_{\mathrm{rel}} = \frac{I_{\mathrm{fl}}(\tau=0) - I_{\mathrm{fl}}(\tau=\infty)}{I_{\mathrm{fl}}(\tau=0)} = \frac{k_{\mathrm{isc}}K}{k_{\mathrm{isc}}K + k_{\mathrm{rel}}}. \quad (10)$$

Since $K < 1$, the relative amplitude is mainly given by the rate constant of the intersystem crossing and the rate of the triplet state relaxation. In Fig. 2a, five decay curves are displayed that differ only in their triplet relaxation rate. It is obvious that if the relaxation of the triplet state is in the same range as the

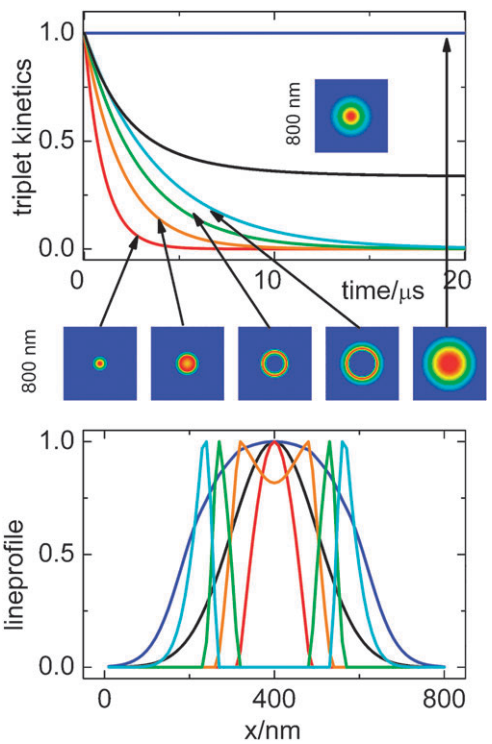

Fig. 1 Images of a point-like fluorescing particle associated with different kinetics. The following parameters were used: $k_{\mathrm{isc}} = 10^7\ \mathrm{s}^{-1}$, $k_{\mathrm{rel}} = 10^5\ \mathrm{s}^{-1}$, $k = 10^9\ \mathrm{s}^{-1}$, $k_{\mathrm{ex}} = 60$ MHz (in the maximum). Upper part: black curve: fluorescence decay curve averaged over the 2D PSF (inset of the upper part). Red, orange, green and cyan curves: decay components with decay times: 1, 2, 3 and 4 µs, respectively. Blue curve: temporally constant offset. Middle part: spatial distribution of the corresponding decay components. Lower part: line profiles of the spatial distributions shown in the middle part: red, orange, green, cyan and blue curve: line profiles associated with the 1, 2, 3 and 4 µs component and the offset, respectively. Black curve: line profile of PSF.

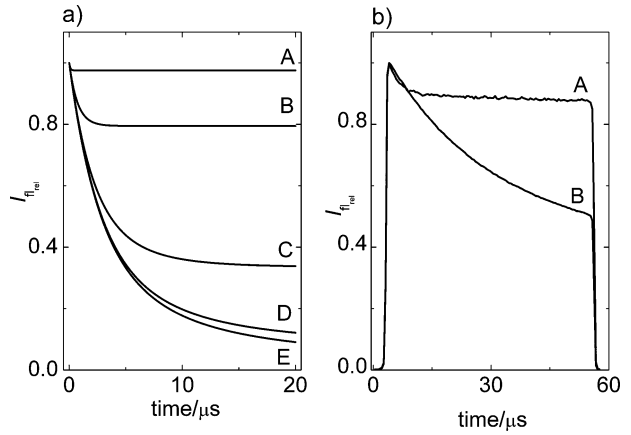

Fig. 2 (a) Theoretical fluorescence decays averaged over the 2D PSF, calculated with the following parameters: $k_{isc} = 10^7\ s^{-1}$, $k = 10^9\ s^{-1}$, $k_{ex} = 60$ MHz (in the maximum) differing in the value of the relaxation rate constant: curves (A–E): $k_{rel} = 10^7\ s^{-1}$, $k_{rel} = 10^6\ s^{-1}$, $k_{rel} = 10^5\ s^{-1}$, $k_{rel} = 10^4\ s^{-1}$, $k_{rel} = 10^3\ s^{-1}$. (b) Decay curves measured in the 1 μM solution of ATTO633 in the presence of oxygen (curve A) and after the oxygen removal (curve B). The excitation intensity at the back aperture of the objective was 0.2 mW.

intersystem crossing rate, the singlet state is quickly recovered, the steady-state amount of triplet is reached rapidly and the amplitude of the kinetics is just a few percent. Such a situation is not favorable for DSOM, since the amplitude of the decay comes close to noise level, which becomes an important issue especially if the amount of photons detected within a time-bin is small. Moreover, all the photons that are detected after the steady state is reached do not contain any information on kinetics and do not contribute to the high resolution image.

The main reason for discussing the amplitudes is the fact that in solutions containing the triplet quencher molecular oxygen (*i.e.*, the relaxation rate is fast and depends on oxygen concentration), the amplitudes of the decays are rather low even at relatively high excitation power (see Fig. 2b). In order to be able to see the larger amplitude of the fluorescence decay, oxygen has to be removed. Except for that, the fluorescence decay can also be modified by employing reduction–oxidation (ROX) systems.[14] The system is usually designed in such a way that it reduces/oxidizes the triplet state and consecutively re-oxidizes/reduces the formed radical anion/cation back to the ground state. Since the rate of both reactions can be tuned by the concentration of the components of the ROX system, the decay can be "tailored" exactly for the purpose of the experiment. ROX were for instance employed in tuning of the off-state of an acceptor in a FRET pair, which causes a non-linearity that can also be utilized in the resolution enhancement of a confocal microscope.[15] A thorough discussion and application of this concept, however, goes far beyond the scope of the present manuscript.

Spatial and temporal resolution. In what follows, we will estimate the limit for the spatial resolution achievable with the given temporal resolution of the acquisition of the fluorescence decays. Let us consider a fluorescing point-like particle localized in the centre of a one-dimensional Gaussian excitation intensity profile. The question is to find the closest distance where the second particle can be localized so that its contribution to the overall fluorescence decay is temporally resolvable with the experiment. We assume that the triplet relaxation rate is sufficiently slowed down and the excitation intensity is moderate, $k_T(\vec{r}) \propto I_{ex}(\vec{r})$. The change of the decay time τ_D ($\tau_D = k_T^{-1}$), *i.e.* of the average time the molecule keeps circulating between the S_0 and S_1 states before it enters the triplet state, close to the middle of the excitation profile can be estimated by: $\tau_D(x) = \tau_D(x_0) + 2\tau_D(x_0)\left(\frac{x-x_0}{\sigma}\right)^2$, where σ is the width of the Gaussian distribution. Based on this rough approximation, we can estimate that the lateral resolution in one dimension R_l scales with the square root of the temporal resolution R_t divided by the decay time $\tau_D(x_0)$:

$$R_l \approx \sigma\sqrt{\frac{R_t}{2\tau_D(x_0)}}. \qquad (11)$$

Similar considerations can be made also for the axial resolution and a Lorentzian distribution of the excitation intensity. For example, in the simulated experiment, shown in Fig. 1, $\tau_D(x_0)$ is approximately 1500 ns, σ equals 200 nm. If the temporal resolution of the fluorescence decay measurement was 100 ns, which is the limit of our camera, the lateral resolution would be around 40 nm. If a similar experiment is done with time-steps of 450 ns, the achievable resolution is around 77 nm, unless either the excitation power is decreased, which slows down the decay (but also reduces the amplitude), or the temporal resolution is increased (which worsens the signal-to-noise ratio).

Choice of the decay times—fitting parameters. The typical way of treating the experimental data, which are given by a series of fluorescence decays measured at each pixel, is fitting the decays to the following model:

$$\mathrm{im}(\vec{r},\tau) = A(\vec{r}) + A_{fast}(\vec{r})\exp\left(-\frac{\tau}{\tau_{fast}}\right) + A_{slow}(\vec{r})\exp\left(-\frac{\tau}{\tau_{slow}}\right), \qquad (12)$$

where $A_{fast}(\vec{r})$ is the high-resolution image corresponding to the fast transition kinetics, described by the short decay time τ_{fast}, and $A_{slow}(\vec{r})$ is the slow kinetic image assigned to the long decay time τ_{slow}. The slow kinetic image is a kind of mathematical iris-like aperture that screens out all the kinetic contributions that are not fast enough. The size of that aperture is given by the choice of τ_{fast} and τ_{slow} and determines the resolution of $A_{fast}(\vec{r})$ and the fraction of photons which are used to create the image.

In order to test the influence of the fitting parameters, the following calculation was performed: a 50 nm rectangular concentration profile was convolved with the 200 nm Gaussian beam according to eqn (4). After the test data had been generated, we fitted them to the model given in eqn (12). Fig. 3 depicts how the choice of the fitting parameters affects the resolution and what fraction of photons participates in the final image. In the upper part of the figure, the impacts of τ_{slow} on $A_{fast}(x)$ are depicted (τ_{fast} is chosen to be the fastest resolvable decay time corresponding to the situation when a point-like fluorescing particle is in the middle of the focus). Analogous to the opening and closing of an iris, the bigger the difference between τ_{fast} and τ_{slow}, the more photons are

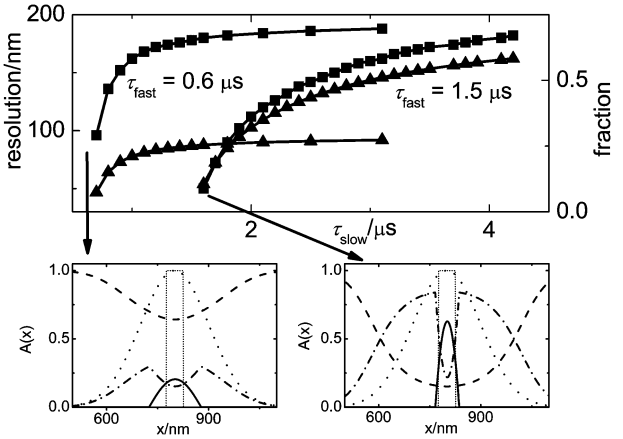

Fig. 3 Upper part: dependence of the spatial resolution (squares) and the fraction of photons (triangles) used for the high-resolved one-dimensional image on the slow component of the fluorescence decays. The parameters used for the calculation: $k = 10^9\ s^{-1}$, $k_{ex} = 60$ MHz (in the maximum), $k_{rel} = 10^6\ s^{-1}$, $k_{isc} = 10^7\ s^{-1}$ ($\tau_{fast} = 0.6$ µs) and $k_{rel} = 10^5\ s^{-1}$ ($\tau_{fast} = 6.4$ µs). Lower part: one-dimensional images of the 50 nm fluorescent source (scanned with the Gaussian light profile (dotted curve) with a half width of 200 nm, which is the original image resolution) associated with the fast (solid curve) and the slow (dot-dashed curve) components and with the temporally constant offset (dashed curve). The spatio-temporal image was calculated according to eqn (4) using a one dimensional 50 nm rectangular profile of concentrations (short dotted curve). The choice of the fast and slow components is marked with arrows.

"transmitted" through the iris to form the high-resolution image. It is obvious that the higher the resolution is, the less photons are involved.

To underline the need of keeping the relaxation rate slow compared to the rate of intersystem crossing, we have chosen two different sets of the photophysical parameters differing in the relaxation rate (see the figure caption). In the case of the faster relaxation rate, the entire fluorescence decay becomes faster ($k_{rel} = 10^6\ s^{-1}$, $\tau_{fast} = 0.6$ µs), but as shown in Fig. 2a (line B), the amplitude is only around 20%, the constant offset is significant and consequently the fraction of photons contributing to the high-resolved image is lower. In the lower part of Fig. 3, for each set of the photophysical parameters, a pair of slow and fast decay times was chosen and the corresponding $A(x)$ (fast, slow and temporally constant contribution) together with the one-dimensional excitation light distribution, which visualizes the original resolution, are shown. The amplitudes of $A(x)$ are normalized to the sum of photons obtained at every point, *i.e.*, the lower part of Fig. 3 shows the relative contribution of all the components at every "scanning step". The further the imaged structure is from the center of the light profile the more the slow and the constant component contributes to the image, while the contribution of the fast one disappears. In the case of the faster triplet relaxation kinetics, there is a noticeable contribution of the slow and the constant component even when the concentration profile is in the middle of the beam. Except for that, also the obtainable spatial resolution reaches the limit set by the temporal resolution of the simulation (100 ns) described by eqn (11), *i.e.*, the size of the original 50 nm structure is no more fully resolvable.

We have introduced an approach that uses only two exponentials for fitting of the decays. Since we are aware of the fact that it is only a rough approximation, we have also tried to introduce the third exponential for fitting of the test data. Width of $A_{fast}(x)$, *i.e.* the resolution, for a given pair of τ_{fast} and τ_{slow}, however, did not almost change by introducing an additional exponential (data not shown). In the case of real data fitting, moreover, the signal-to-noise ratio comes into play. Using more exponentials therefore worsens the resolution rather than improve it, since the high-resolved image becomes noisier.

Experiments done on the planar bilayers

A supported lipid bilayer (SLB) is a few-nanometre thick layer that is, in our experiments, fluorescently labeled with a certain fraction of dye-labeled lipid molecules. By scanning the layer along the propagation axis of the laser focus, the vertical resolution of our imaging setup can be determined. The advantage of using SLBs as a model system for demonstrating the applicability of the DSOM concept is the fact that even though irreversible photobleaching always occurs to some extent, the dye in the bilayer is constantly refreshed due to lateral diffusion. Therefore, the fluorescence decay at each pixel can be measured repeatedly and the obtained data have a high signal-to-noise ratio and can be well used for the exponential fitting. It has to be mentioned that the fluorescence decay at each position relative to the center of the focus is averaged over the whole illuminated area. Therefore, the change in kinetics along the z-axis is not as steep as it would be if a point-like source had been used. The question to be answered is whether the resolution improvement that is measured on such a model system can be related to the improvement that would be obtained for a point source. To compare these two situations, we have approximated the illuminated intensity distribution by a Gaussian–Lorentzian distribution:[16]

$$I_{ex}(x,y,z) = \frac{1}{w^2(z)}\exp\left[-\frac{2}{w^2(z)}(x^2+y^2)\right], \qquad (13)$$

where

$$w^2(z) = w_0^2\left[1+\left(\frac{\lambda_{ex}z}{\pi w_0^2 n}\right)^2\right]. \qquad (14)$$

λ_{ex} is the excitation wavelength, n is the refractive index, and w_0 is the $1/e^2$-radius of the 2D Gaussian distribution in the focus. Dependences of the achievable axial resolution on the slow decay component were calculated both for the point source and for the planar source—membrane (see Fig. 4). Apparently, in both the cases the spatial resolution is only limited by the temporal resolution of the experiment with respect to the transition kinetics, as already discussed before. However, even though the resolution enhancement is the same for both the considered geometries, the difference lies in the photon fraction that is used to form the image. Whereas in the case of the point source, all the fluorescence comes only from the center of the beam, in the case of the membrane, additional light comes from non-axial parts of the plane and contributes

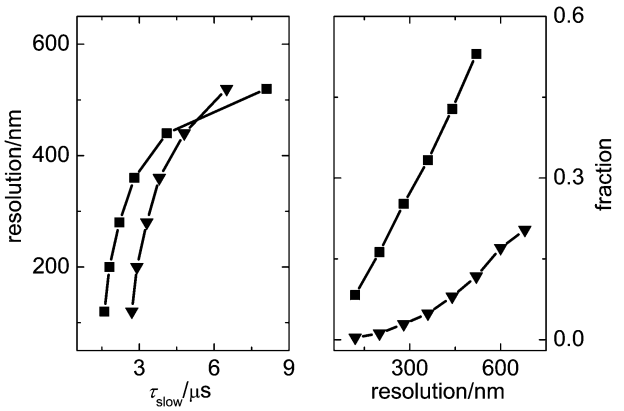

Fig. 4 Left: dependence of the axial resolution on the chosen long decay time for the point (squares) and planar (triangles) source. Right: dependence of the photon fraction on the desired axial resolution for the point (squares) and planar (triangles) source. The short decay time was 1500 ns. The width of the used Lorentzian distribution was approximately 710 nm. The width of the 2D Gaussian in the focal plane was 200 nm. The following parameters were chosen similarly to the previous calculations: $k = 10^9\ s^{-1}$, $k_{ex} = 60$ MHz (in the maximum), $k_{rel} = 10^5\ s^{-1}$, $k_{isc} = 10^7\ s^{-1}$.

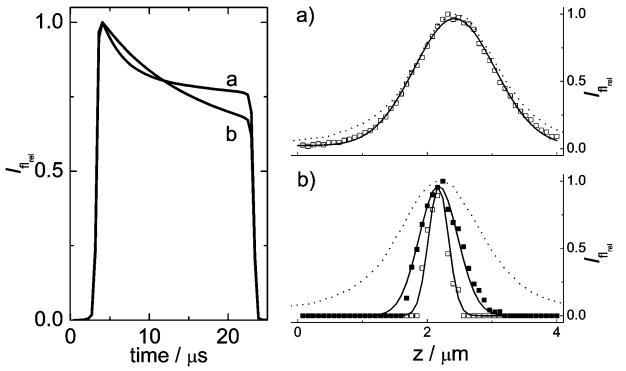

Fig. 5 Left: fluorescence decays measured on the supported lipid membrane labeled with ATTO633 bound to a fraction of lipids. Experiment was done in the presence of oxygen (line(a)) and in the absence of oxygen (line(b)). Right: (a) and (b) open squares: high resolved z-profiles obtained with DSOM, full squares: different choice of the fitting parameters giving medium resolution, dotted curves: z-profiles obtained without DSOM at low power, solid curves: Gaussian fits of the appropriate data. We analyzed 50 decays along the z-axis with the step of 80 nm. In order to have high-quality data, every analyzed decay was obtained as an average of 12 000 measurements with a delay of 3 ms, which is necessary for membrane recovery and for reading of the camera. The entire acquisition took around 6 minutes. The excitation power at the back aperture of the objective was around 0.2 mW.

to the slower kinetics, thus increasing the fraction of photons that are screened out. Therefore, the membrane measurement requires overall more photons compared to the point source to have the same data quality.

Experimentally, we have applied DSOM for the following two cases:

(a) The membrane was in the buffer solution containing oxygen.

(b) The membrane was flushed with the buffer where oxygen was depleted.

In Fig. 5, the fluorescent decays corresponding to the above mentioned situations are displayed. In the case with oxygen (line (a)), the amplitude of the decay is decreased by the fast recovery of the singlet state. When the oxygen is depleted, the amplitude increases since the triplet lifetime becomes larger. Surprisingly, after oxygen removal, the transition from the singlet to the triplet state slows down. (Compare Fig. 2a, where only triplet relaxation rate changes, with lines (a) and (b) in Fig. 5, left. A similar phenomenon can also be seen in solution in Fig. 2b.) A possible explanation for this behavior is that the depopulation of the excited singlet state is not only caused by the transition to the triplet but also by fast direct reaction with oxygen, which may for example, form molecular complexes with the dye. It has to be pointed out that this seems to be specific for ATTO633, since the fluorescence decays of ATTO655 and ATTO647 in solution in the presence and absence of oxygen behave as expected (data not shown). We are aware of the fact that our explanation is rather speculative. However, the photophysics of ATTO633 is not the aim of this manuscript and thus, we take the advantage of this behavior to show an example of the process that cannot be monitored with the used temporal resolution. Actually, when inspecting individual fluorescence decays of the de-oxygenized sample around the centre of the focus, we cannot see any changes in the kinetics. Consequently, after fitting of the data, no matter how the fitting parameters are chosen, no significant resolution improvement is observed (Fig. 5a). Apparently, most of the kinetics is faster than 450 ns, which was the temporal resolution of our experiment. When oxygen is depleted, there are observable changes in the kinetics in the axial direction.

In Fig. 5b, two different high-resolution intensity profiles are depicted for two different choices of the slow kinetics. The decay time measured when the membrane was in focus was used as the short decay time ($\tau_{fast} = 9$ μs). τ_{slow} was chosen to differ from τ_{fast} by the temporal resolution of our experiment, and then still increased until the intensity profile was sufficiently smooth (open squares, $\tau_{slow} = 10.8$ μs). In this way, the standard axial resolution represented by the dotted line was improved from 1250 nm to 300 nm, *i.e.* by a factor 4. When increasing τ_{slow} further to 12 μs, the z-profile broadens yielding a resolution of 600 nm.

Experiments done on fluorescently labeled polystyrene beads

Having demonstrated that DSOM works well for a planar system, the approach was tested on labeled polystyrene beads. It has to be pointed out that the method requires triplet state formation and subsequent dwelling of the fluorophores in the triplet state, which has to be long enough so that the amplitude of the fluorescence decay is sufficiently large. Since the triplet state is rather reactive, the most critical factor for applying DSOM is photobleaching. The problem can be minimized if the acquisition time is reduced and a compromise between photobleaching and data quality can be found. In the case of beads, the dye is incorporated in a glassy polymer matrix, which prevents the fluorophores in the triplet state to be depopulated by oxygen, thus no oxygen depletion is required. It has to be kept in mind that in the oxygen-free environment,

the lifetime of the triplet state is significantly increased and therefore a delay is needed between two consequent decay measurements that allows for relaxation of all molecules to the ground-state. In our case, 40 ms was sufficient. Fig. 6a and b show a typical example, where the width of the point spread function is reduced approximately by a factor of 1.8. The PSF image corresponding to conventional diffraction-limited imaging was reconstructed from the beginning of the fluorescence decays before the triplet state formation occurred. (The expansion of the PSF due to the saturation between the S_0 and S_1 state[4] can be neglected at the used laser power.) The image is slightly elongated in one direction because of laser polarization. As τ_{fast}, the decay time in the center of the original confocal image was chosen (τ_{fast} = 1800 ns). τ_{slow} was chosen similarly as in the case of the experiments with SLBs, *i.e.* starting with the time that differs at least by the temporal resolution of the measurement (100 ns) and increasing it so that the 2-D Gaussian fit of the high resolved image gave the lowest width, we ended with τ_{slow} = 2000 ns. Usually, if the two decay times are not separated enough, the high resolved image is noisy. By further increase of the slow time, the images becomes smoother, but the resolution gets worse.

Time-modulated excitation—"integrative" mode

The use of an EMCCD camera in "line-shifting" mode as described in the Experimental section allows for combining high detection efficiency and dynamic range of the camera with relatively high temporal resolution. However, the temporal resolution used for fluorescence decay acquisition is anyway limited by the speed with which the camera shifts the lines and therefore it is not sufficiently versatile. It has been shown that the fluorescence decay can be also measured by modulating the length of the excitation pulses.[17] Since the fluorescence decay at a given excitation rate can be described as: $I_{fl} = A + B\exp(-k_T\tau)$, the dependence of the average fluorescence intensity on the length of the excitation pulses T follows the relation:

$$I_{fl} = \lim_{T\to 0}\frac{1}{T}\int_0^T (A + B\exp(-k_T\tau))\mathrm{d}\tau = A + B\exp(-k_T T). \quad (15)$$

In other words, the temporally resolved fluorescence decay measurement is achieved by applying pulses of different length and measuring the average fluorescence intensity. In the case of the beads, this approach would be rather lengthy because of the long relaxation from the triplet state. However, in systems where the lifetime of the triplet state can be tuned, this approach might become more useful. To demonstrate that this idea works, we have used the decays from the experiment depicted in Fig. 4 and integrated them over increasingly logarithmically spaced time intervals. The obtained dependences were subsequently fitted similarly to the "line-shifting" approach, which resulted in Fig. 6c. Apparently, the obtained resolution improved as compared to the standard diffraction-limited image. However, it is slightly worse than that obtained with the direct acquisition of the decays, probably as a result of averaging.

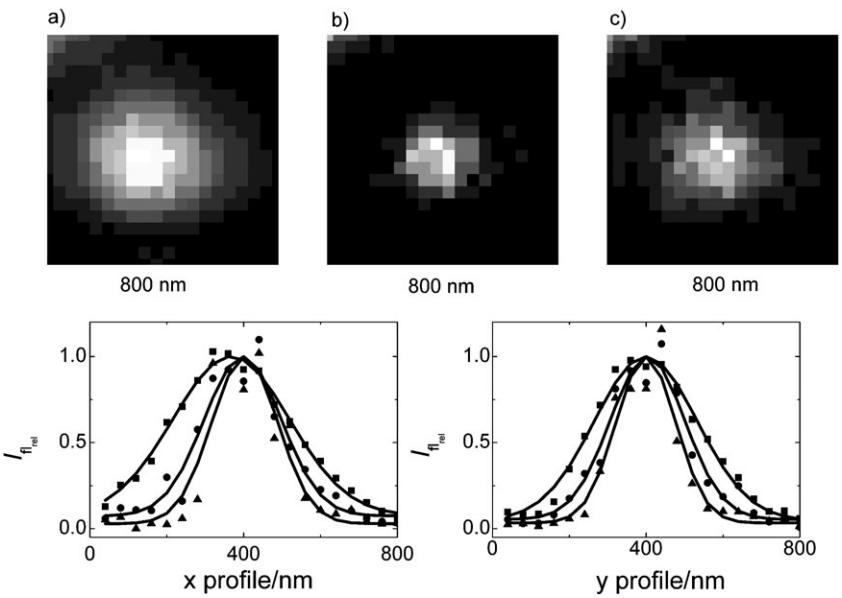

Fig. 6 Upper part: (a) point spread function (PSF) reconstructed from the fluorescence intensity at the beginning of the decays measured at every pixel, *i.e.*, prior to relaxation to the triplet state (diffraction-limited resolution), (b) PSF obtained *via* DSOM, (c) PSF obtained *via* DSOM in the "integrative" mode. Original images were acquired with a pixel size of 10 nm, *i.e.* 80 × 80 pixels. At each pixel, two 10 μs decay curves were measured. Between two consecutive measurements, a 40 ms delay was introduced to let the formed triplet state relax back to the singlet ground state. In order to reduce noise, after fitting the decays using eqn (7) with fixed decay times, fractions associated with the decay times were binned in 4 pixel × 4 pixel manner. The excitation intensity at the back aperture of the objective was around 20 μW, the entire acquisition time was approximately 9 minutes. Lower part: x and y line profiles corresponding to the PSFs in the upper part: (a) squares, (b) triangles, and (c) circles. Half widths of the line profiles obtained from the Gaussian fitting: x profile: (a) 303 nm, (b) 172 nm, (c) 200 nm; y profile: (a) 268 nm, (b) 156 nm, (c) 194 nm.

Experimental

Confocal microscopy

The experiments were performed with a home-built optical setup based on the inverted microscope IX71 (Olympus, Hamburg, Germany). The excitation light (488 nm line of Ar-ion laser or 633 nm He–Ne laser) passes through an acousto-optical tunable filter (AOTF) and an acousto-optical modulator (AOM) (AOTFnC-400.650 and MT200-A0,5-VIS, AAOptoelectronic, Orsay, France). The AOTF selects the wavelength and intensity, and the AOM creates sharp short (microseconds) rectangular pulses (rise time below 50 ns). The intensity modulated laser beam is coupled into a single-mode polarization-maintaining optical fiber (LINOS Photonics, Goettingen, Germany) for spatial mode filtering. Re-collimation is done with an air-spaced objective (UPLSAPO 4X, Olympus), and the collimated laser beam enters the back port of the microscope body. The microscope itself contains the standard confocal part consisting of a z488rdc or z635 dichroic mirror (Chroma, Rockingham, VT), a water immersion objective (UPLSAPO 60×, Olympus), 3D sample scanning stage (PIMars XYZ NanoPositioner, 200 × 200 × 200 μm, PI, Karlsruhe, Germany), 50 μm diameter pinhole placed at the focal plane of the left camera port, a recollimation lens, and an HQ515/50 or HQ685/80 emission filter (Chroma). In contrast to standard confocal setups, the detection unit is an EMCCD camera (DU-860D-CS0-#BV iXon 128 × 128 pixels, Andor, Belfast, United Kingdom). The projected image of the pinhole on the EMCCD is made smaller by a factor of 5 to fit into a single pixel (24 μm × 24 μm) close to the bottom of the light sensitive part of the chip. A small portion of light leaks to the nearest pixels and smears the measured time profile. All optomechanical components were bought from Thorlabs (Newton, NJ).

The fast microsecond dynamics is captured using the so called image shifting mode. The excitation light is switched off until the camera starts to read out an image using a frame transfer mode. As the blank image starts moving down the chip, excitation is switched on and the time evolution of the signal is inscribed along a vertical direction on the EMCCD chip. The time resolution is given by the available camera vertical line clock (from 88 to 450 ns), the maximum number of time points is given by number of pixels on the camera chip (128). We usually used 450 ns vertical clock and 128 pixels for measuring decays lasting 10 to 20 μs. Afterwards, the shifted image is binned 3 × 1 and read out in a standard way using the EM register. For each horizontal line (time point), the fluorescence signal that is contained in a single binned pixel is corrected for variable camera background using non-illuminated pixels in that line. It takes in total 2 ms to record and store one 128 pixel decay, which sets the speed limit for scanning.

An important part of the setup is a proper synchronization of the excitation, scanning and detection units. The master unit is the scanner, which triggers the EMCCD camera. To keep precise timing, the camera sends trigger (fire) pulses to a DAQ board (PCIe 6259, National Instruments, Austin, TX), which modulates the AOTF, and with TTL pulses triggers a fast waveform generator (DA4300, Acquitek, Massy, France) which modulates the AOM.

The EMCCD detection is used for its high dynamic range (from single photon to thousands per time point), linearity of response, sensitivity and reasonable time resolution in the image shifting mode. Standard SPAD modules are unable to capture more than 1 photon per dead time (*ca.* 200 ns), which makes them unusable for the experiments presented here. On the other side, PMT modules in the analogue regime are fast enough, but have much lower detection efficiency.

Sample preparation

Supported lipid bilayers. Chloroform solutions containing 1 μmol of 1,2-dioleoyl-*sn*-glycero-3-phosphocholine and 4 nmol of ATTO-633 (ATTO-TEC, Siegen, Germany) labeled 1,2-dioleoyl-*sn*-glycero-3-phosphoethanolamine (Avanti Polar Lipids, Alabaster, AL)[18] were mixed, chloroform was evaporated under vacuum and the lipid film was resuspended in 1 mL of buffer containing 10 mM HEPES, 150 mM NaCl and 1 mM EDTA (pH = 7.4). The aqueous lipid solution was sonicated with the tip sonicator for 20 min and the solution of formed small unilamellar vesicles was pipetted into a 10 fold excess of calcium containing buffer solution (10 mM HEPES, 150 mM NaCl and 1 mM $CaCl_2$) in a glass cuvette. After 10 min of incubation, the bilayer was formed on the surface of the cuvette and the remaining vesicles were flushed away with the excess of calcium containing buffer.[19] For the measurements in oxygen free solution, the calcium containing buffer was enriched with GODCAT oxygen scavenger, *i.e.*, the final buffer contained 10 nM glucose oxidase, 1.5 μM catalase and 56 mM glucose. The cuvette containing SPBs was flushed with an excess of the oxygen free buffer. If not mentioned otherwise, all the used chemicals were ordered from Sigma-Aldrich, Saint Louis, MO.

Polystyrene beads. Yellow-green 100 nm carboxylate-modified microspheres were obtained from Invitrogen (Carlsbad, CA), sonicated and dispersed on the glass cover slip.

Conclusion

In this manuscript we presented an experimental realization of dynamic saturation optical microscopy (DSOM)—a new technique for super-resolution imaging, which has been so far proposed only theoretically.[13] The main idea behind DSOM relies on introducing a temporal dependence of switching between bright and dark states of the fluorophores into an imaging procedure. We show that the kinetics of the transition from the on-state to the off-state depends exponentially on the excitation intensity, which allows for theoretically unlimited spatial resolution. In the real experiment, the spatial resolution was limited by the temporal resolution used for the acquisition of the kinetics, number of photons, and, naturally, also by the scanner stability and the size of the structures being observed. Theoretically, the method can be applied to any system which undergoes a transition between two states, for example to photoswitchable proteins, but also to any organic dye molecule that exhibits transition to the triplet state, which was the main issue of this contribution.

In the manuscript, we discuss which requirements have to be fulfilled so that DSOM can be applied, namely the fact that

dwelling time of molecules in the dark state has to be sufficiently long. Further, we estimated spatial resolution that can be obtained with the Gaussian light profile and given temporal resolution.

In the theoretical introduction, it is shown that the spatio-temporal image, *i.e.* the image consisting of the kinetic measurement at every pixel, can be developed into an infinite series of images associated with a certain kinetic rate. The one assigned to the fastest kinetics corresponds to the high-resolved image. In order to obtain the amplitude of the fastest kinetics at every pixel, we have decided to fit the data with a model that assumes two kinetic components only, the fast and the slow one. We have tested this approach on the model data, realized that is sufficient and show that varying of the slow decay constant allows for establishing compromise between the resolution and the data quality, namely the photon fraction that is used to construct the image.

We tested DSOM on two model systems, supported lipid bilayers (SLBs) and polystyrene beads loaded with a fluorescent dye. When using SLBs, the photobleached fluorescence dye is instantly being recovered by diffusion, thus minimizing photobleaching problems. The experiments demonstrate that DSOM is a method that can indeed substantially improve the resolution, in our case by a factor of four. The measurements on the polystyrene particles demonstrated that even though the photostability becomes an issue, the resolution improvement is still considerable.

The main advantage of employing triplet state formation kinetics for resolution enhancement is the fact that intersystem crossing is a feature common to most fluorophores used in fluorescence microscopy. The main disadvantage of triplet state formation is its fast recovery *via* oxygen-mediated relaxation. This can be circumvented by depleting oxygen with an oxygen scavenger or by quickly depopulating the triplet state with a suitable ROX system.[14] In the case of the polystyrene beads, the dye was embedded in a glassy polymer matrix and thus, no special treatment was required.

Eventually, it has to be stressed that DSOM is a method that is technically simple and the treatment of the data is straightforward and reasonably robust.

In summary, even though currently DSOM cannot compete with already established super-resolution techniques, it has a high potential in spatial resolution. Using the triplet state as the dark state imposes requirements on the triplet relaxation kinetics, which in the presence of oxygen is usually insufficiently slow. However, several approaches are known that allow for controlling triplet or generally dark state lifetimes.[20] Therefore, the main problem comes from the fact that even though the lifetime of the triplet state can be tuned, it is always important that the fluorophore stays either in the triplet state or in the state of radical anion or cation long enough ($\sim$100 μs) to reach reasonable amplitude of the fluorescence decay. Unfortunately, such a time can be already long enough for certain photobleaching processes to occur. This means that not only the dye itself but also its chemical microenvironment plays a role in successfully applying DSOM.

Finally, we would like to point out that most of the problems that have arisen when using the triplet state as the dark state would probably disappear if photoswitchable proteins are involved.

Acknowledgements

JH acknowledges the support of the Ministry of Education of the Czech Republic *via* grant LC06063 and MH acknowledges the Czech Science Foundation EUROMEMBRANES (MEM/09/E006). AB would like to acknowledge financial support of the Academy of Sciences of the Czech Republic *via* grant KJB400400904. JE acknowledges financial support by the Human Frontier Science Program (RGP46/2006) and by the German Federal Ministry of Education and Research (FKZ 13N9236).

References

1 M. G. L. Gustafsson, *J. Microsc.*, 2000, **198**, 82–87.
2 R. Heintzmann, T. M. Jovin and C. Cremer, *J. Opt. Soc. Am. A*, 2002, **19**, 1599–1609.
3 K. Fujita, M. Kobayashi, S. Kawano, M. Yamanaka and S. Kawata, *Phys. Rev. Lett.*, 2007, **99**, Article Nr. 228105.
4 J. Humpolíčková, A. Benda and J. Enderlein, *Biophys. J.*, 2009, **97**, 2623–2629.
5 E. Rittweger, K. Y. Han, S. E. Irvine, C. Eggeling and S. W. Hell, *Nat. Photonics*, 2009, **3**, 144–147.
6 S. W. Hell, R. Schmidt and A. Egner, *Nat. Photonics*, 2009, **3**, 381–387.
7 M. J. Rust, M. Bates and X. W. Zhuang, *Nat. Methods*, 2006, **3**, 793–795.
8 B. Huang, W. Q. Wang, M. Bates and X. W. Zhuang, *Science*, 2008, **319**, 810–813.
9 M. Bates, B. Huang, G. T. Dempsey and X. W. Zhuang, *Science*, 2007, **317**, 1749–1753.
10 S. van de Linde, R. Kasper, M. Heilemann and M. Sauer, *Appl. Phys. B: Lasers Opt.*, 2008, **93**, 725–731.
11 M. Heilemann, S. van de Linde, M. Schuttpelz, R. Kasper, B. Seefeldt, A. Mukherjee, P. Tinnefeld and M. Sauer, *Angew. Chem., Int. Ed.*, 2008, **47**, 6172–6176.
12 T. Dertinger, R. Colyer, G. Iyer, S. Weiss and J. Enderlein, *Proc. Natl. Acad. Sci. U. S. A.*, 2009, **106**, 22287–22292.
13 J. Enderlein, *Appl. Phys. Lett.*, 2005, **87**, Article Nr. 094105.
14 J. Vogelsang, R. Kasper, C. Steinhauer, B. Person, M. Heilemann, M. Sauer and P. Tinnefeld, *Angew. Chem., Int. Ed.*, 2008, **47**, 5465–5469.
15 J. Vogelsang, T. Cordes, C. Forthmann, C. Steinhauer and P. Tinnefeld, *Nano Lett.*, 2010, **10**, 672–679.
16 A. G. Palmer and N. L. Thompson, *Appl. Opt.*, 1989, **28**, 1214–1220.
17 T. Sandén, G. Persson, P. Thyberg, H. Blom and J. Widengren, *Anal. Chem.*, 2007, **79**, 3330–3341.
18 M. Štefl, A. Kulakowska and M. Hof, *Biophys. J.*, 2009, **97**, Lo1–Lo3.
19 A. Benda, M. Benes, V. Marecek, A. Lhotsky, W. T. Hermens and M. Hof, *Langmuir*, 2003, **19**, 4120–4126.
20 J. Vogelsang, T. Cordes, C. Forthmann, C. Steinhauer and P. Tinnefeld, *Proc. Natl. Acad. Sci. U. S. A.*, 2009, **106**, 8107–8112.